Nonisovalent Si-III-V and Si-II-VI alloys: Covalent, ionic, and mixed phases

Joongoo Kang,[1,*] Ji-Sang Park,[2] Pauls Stradins,[3] and Su-Huai Wei[4,†]
[1]*Department of Emerging Materials Science, DGIST, Daegu 711-873, Korea*
[2]*Argonne National Laboratory, Argonne, Illinois 60439, USA*
[3]*National Renewable Energy Laboratory, Golden, Colorado 80401, USA*
[4]*Beijing Computational Science Research Center, Beijing 100094, China*
(Received 10 April 2017; published 13 July 2017)

Nonequilibrium growth of Si-III-V or Si-II-VI alloys is a promising approach to obtaining optically more active Si-based materials. We propose a new class of nonisovalent Si_2AlP (or Si_2ZnS) alloys in which the Al-P (or Zn-S) atomic chains are as densely packed as possible in the host Si matrix. As a hybrid of the lattice-matched parent phases, Si_2AlP (or Si_2ZnS) provides an ideal material system with tunable local chemical orders around Si atoms within the same composition and structural motif. Here, using first-principles hybrid functional calculations, we discuss how the local chemical orders affect the electronic and optical properties of the nonisovalent alloys.

DOI: 10.1103/PhysRevB.96.045203

I. INTRODUCTION

Silicon is the "workhorse" semiconductor of the electronic age because of its desirable material properties such as high quality of its surface oxide, high purity, and well-established growth and doping technologies. Because of its indirect band gap, however, silicon is not ideal for optoelectronic applications. Nevertheless, bulk silicon is still widely used as a light-absorbing material in photovoltaic cells with a total market share of above 90% [1]. Obtaining optically more active Si-based materials is a considerable challenge that holds great potential for optoelectronics and solar energy conversion with silicon. Massive efforts have been made to search for new Si-based materials that have a more direct and/or increased band gap to improve solar conversion efficiency and optoelectronic properties [2–12].

Of the progress that has been made in recent years, one of the most promising methods is to make use of molecular precursors for the nonequilibrium growth of nonisovalent Si_3AlP alloys [5–8]. As a hybrid of diamond cubic Si and zinc blende AlP, the Si_3AlP alloy is lattice-matched to Si because the parent bulk phases have nearly identical lattice constants. If the Al-P-Si_3 tetrahedral units, which are generated from the molecular $P(SiH_3)_3$ reacting with Al atoms, were stable in synthesis conditions, Si_3AlP would exclusively contain isolated Al-P "pairs" in the host Si matrix. As the previous work [8] elegantly demonstrated, however, the decomposition of the Al-P-Si_3 units leads to the formation of Si_3AlP containing Al-P "chains" as a new structural motif, as well as the Al-P pairs. The synthesized Si_3AlP shows higher absorption than bulk Si in the visible range, but the strength of the absorption is substantially lower than the theoretical result for the models based on the Al-P pairs.

Motivated by the experimental finding of the Al-P atomic chains as a new structural motif for the Al-P component, we consider the possibility of new Si-Al-P phases that contain solely the Al-P chains as densely packed as possible in the host Si matrix. The search for the phases exclusively based on the Al-P chains is a strategy for going beyond Si_3AlP in terms of the composition of AlP and thus potentially achieving higher band gap. In this work, we identified a variety of Si_2AlP phases (i.e., half-and-half Si and AlP) that are constructed from the Al-P chains and the complementary Si-Si chains as the building units (Fig. 1). The newly identified Si_2AlP provides a unique material system with tunable local chemical orders around Si atoms within the same composition and structural motif. Thus, it can be used for systematically studying different prototypes of nonisovalent alloys with "covalent," "ionic," and "mixed" local environments. Because ZnS ($a = 5.41$ Å [13]) also has a nearly same lattice constant a as for Si (5.43 Å) and AlP (5.46 Å), we also considered the Si_2ZnS alloys and found a direct-band-gap phase with strong absorption in the visible range.

II. RESULTS AND DISCUSSION

To investigate the effects of different local chemical orders on the optoelectronic properties of Si_2AlP and Si_2ZnS, we performed first-principles density functional calculations using the Vienna *Ab Initio* Simulation Package (VASP [14]). Our calculations employed the projector augmented wave method [15,16] with an energy cutoff of 280 eV for the plane-wave part of the wave function. Throughout the paper, the results were obtained by using the HSE hybrid density functional [17] except if otherwise indicated.

Structures of Si_2AlP alloys. To describe the Si-Al-P alloys considered in this work, we introduce two indices, x and y, which can vary from 0 to 1. The index x denotes the alloy composition as $(Si_2)_{1-x}(AlP)_x$. For example, the x values of Si_3AlP and Si_2AlP are 0.4 and 0.5, respectively. The index y describes local chemical orders around Si atoms in Si_2AlP, which can take one of the three bond configurations: (i) Si atom bonding with two Si atoms and one Al and one P (Si–Si_2AlP), (ii) Si atom bonding with two Si atoms and two Al atoms (Si–Si_2Al_2), and (iii) Si atom bonding with two Si atoms and two P atoms (Si–Si_2P_2). This is unlike the case of Si_3AlP, for which the proposed crystal structure contains only Si–Si_2AlP [6]. For Si_2AlP, the index y is then defined by the ratios of the different local chemical orders as in $(1-y)$Si–$Si_2AlP + y/2$ Si–$Si_2Al_2 + y/2$ Si–Si_2P_2. The same definition of y will

*joongoo.kang@dgist.ac.kr
†suhuaiwei@csrc.ac.cn

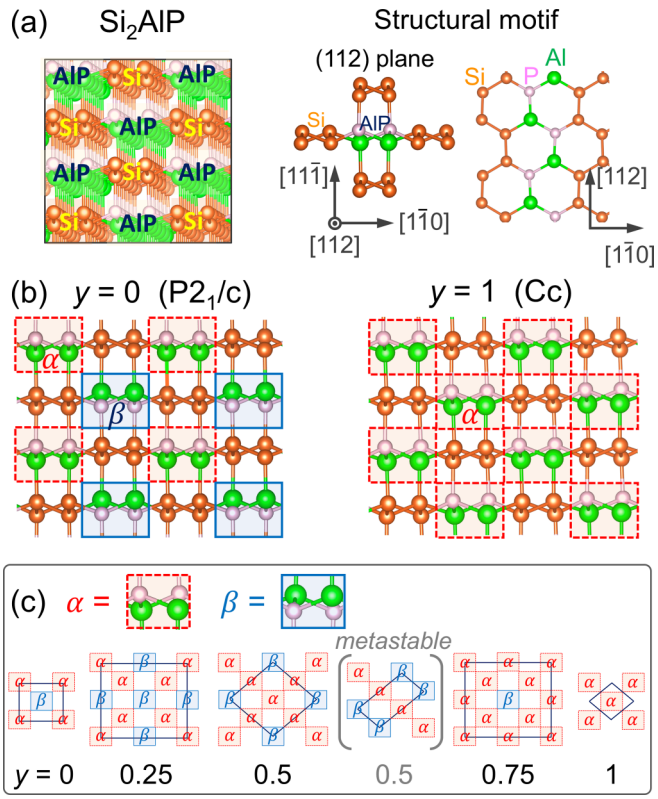

FIG. 1. Atomic structures of Si_2AlP for covalent, ionic, and their mixed phases. (a) In Si_2AlP, the Si-Si and Al-P atomic chains form an ordered pattern to incorporate the large fraction of AlP in the host Si matrix (left panel). In the right panel of (a), the structural building units of Si_2AlP are shown from two perspectives: top view (left) of the (112) plane and side view (right) showing the Al-P and Si-Si chains extending along the [112] direction. (b) Two ordered Si_2AlP phases with $y = 0$ (left) and $y = 1$ (right). Each Al-P chain is labeled by α (dashed rectangle) or β (solid rectangle) depending on its electric dipole direction with respect to the [112] direction. (c) Mixed phases of Si_2AlP with intermediate values of y. The periodicity (unit-cell projection) of each phase is denoted by a parallelogram.

also be used for Si_2ZnS, in which the cations and anions in Si_2AlP change to Zn and S accordingly.

Figure 1 presents the atomic structures of Si_2AlP that are constructed from the Si-Si chains and the Al-P chains as the building units. Each of the atomic chains extends along the [112] direction (as labeled in diamond cubic structure). The Si-Si and Al-P chains form an ordered pattern to incorporate the high fraction of AlP in the host Si matrix [Fig. 1(a)]. The (112) plane, which is perpendicular to the constituent atomic chains, can be regarded as having two sublattices of Si-Si and Al-P sites. Each Al-P chain can take two different orientations (labeled by α and β) with its electric dipole either parallel or antiparallel to the [112] direction [Fig. 1(b)]. The y value of Si_2AlP varies from 0 to 1, depending on how α and β occupy the sublattice sites of the Al-P chains. Regardless of the y value, the local chemical orders around Al and P atoms are the same as Al–Si_2P_2 and P–Si_2Al_2, respectively.

The two extreme phases of Si_2AlP on the scale of y are shown in Fig. 1(b). The phase with $y = 0$ (y_0 for short) has the space group $P2_1/c$ and contains 16 atoms in the primitive unit cell. For the phase with $y = 1$ (y_1; space group Cc), the unit-cell size is reduced to half the unit-cell size of y_0, because the y_1 phase consists of the Al-P chains of the same type. The atomic coordinates of the y_0 and y_1 phases are listed in Table I. The Si atoms in the y_0 phase have the identical local environment as Si–Si_2AlP, and they are "charge neutral" in the sense that each Si atom bonds to one anion and one cation. For the y_1 phase, however, half of the Si atoms are "anions" of the Si–Si_2Al_2 type, while the other half are "cations" of the Si–Si_2P_2 type.

Besides the covalent y_0 and the ionic y_1, we also consider the mixed phases with intermediate y values to study the effects of the local chemical orders around Si atoms on the electronic and optical properties of Si_2AlP and Si_2ZnS [Fig. 1(c)]. The key questions that will be addressed are which phase is more stable among the various phases with different y values and how the electronic band-edge energies and characters depend on the local chemical orders. We discuss the theoretical framework for understanding the electronic properties of the alloys. Finally, we explore whether the nonisovalent alloys, Si_2AlP or Si_2ZnS, are better light absorbers than Si, with stronger visible range absorption.

Stability of the nonequilibrium Si-Al-P phases. Figure 2(a) compares the relative stabilities of Si_2AlP with different y. The y_0 structure has lower intracell energy than y_1 because the former locally satisfies the octet rule around each Si atom. The alternating occupation of α and β for the Al-P sites in the y_0 phase can further lower the dipole-dipole interactions between the chains and release the strain energy of the alloy. The y_1 structure, however, can have lower Coulomb interaction energy between the anion-type Si atoms and the cation-type Si atoms. It turns out that the net effect is the higher stability of the y_0 phase by 14 meV/atom. The relative stability is concave in energy between $y = 0$ and $y = 1$, indicating that the two

TABLE I. The structural parameters of Si_2AlP phases that are obtained by using the HSE hybrid calculations: symmetry, lattice parameters (in Å), and angles (°) of a unit cell, and Wyckoff positions. The unit-cell size of the y_1 phase given below is twice the size of its primitive cell.

	$y = 0$	$y = 1$
Symmetry	$P2_1/c$	Cc
a, b, c	6.75, 7.74, 6.69	7.75, 7.75, 6.66
α, β, γ	90, 109.48, 90	90, 125.39, 90
Si_1	0.67339, 0.62630, 0.81900 (4e)	0.38325, 0.13285, 0.00016 (4a)
Si_2	0.79709, 0.62756, 0.19207 (4e)	0.25327, 0.37742, 0.75028 (4a)
Al_1	0.81394, 0.12357, 0.17990 (4e)	0.24690, 0.12829, 0.24975 (4a)
P_1	0.68556, 0.12273, 0.80028 (4e)	0.36658, 0.38364, 0.49981 (4a)

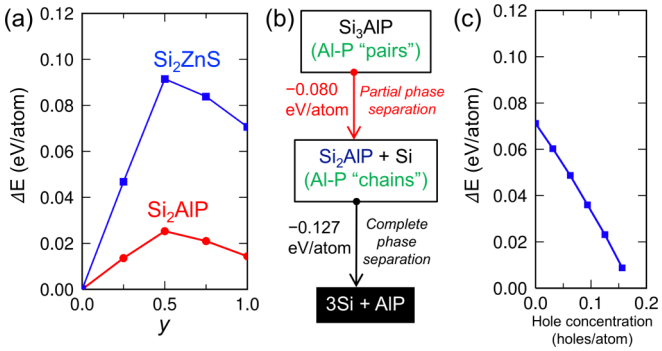

FIG. 2. Stability of the nonequilibrium Si-Al-P phases. (a) Dependence of the stability of Si_2AlP alloys on the structural index y. The stabilities of the phases with nonzero y are shown with respect to that of the phase with $y = 0$. For comparison, the results for Si_2ZnS are also included. (b) Schematic representation of the relative stabilities of the Si-Al-P systems. (c) Dependence of the energy difference for the y_1 and y_0 phases of Si_2ZnS on the hole concentration.

extreme phases, y_0 and y_1, are energetically preferred than the intermediate phases. For comparison, we also present the results for Si_2ZnS in Fig. 2(a). For both Si_2AlP and Si_2ZnS, we found the same trend in the stabilities of alloys but with much-enhanced energy differences for Si_2ZnS because of its higher charge polarization and hence the larger Coulomb interaction.

We also examined the relative stability of Si_3AlP ($x = 0.4$) and Si_2AlP ($x = 0.5$) by considering the partial phase separation of Si_3AlP to Si_2AlP and bulk Si [Fig. 2(b)]. The Si_2AlP phase is energetically more stable than the metastable Si_3AlP by 80 meV/atom. Because of the different Al-P bond distributions (pairs vs chains), the partial phase separation of Si_3AlP is driven by the energy gain in the Coulomb energy between the Al cations and the P anions. If Si_2AlP undergoes a further phase separation to bulk Si and bulk AlP, the total energy is lowered by 127 meV/atom.

Effects of the local chemical orders on the band-edge energies of Si_2AlP and Si_2ZnS. The y_0 and y_1 phases of Si_2AlP are pseudo-direct band-gap semiconductors with the valence-band edge at the Γ point. The band gap of y_0 is calculated to be 1.29 eV (HSE06) and 1.28 eV (G_0W_0), and the band gap of y_1 is 1.44 eV (HSE06) and 1.42 eV (G_0W_0). Figure 3(a) shows how the band-edge energies of Si_2AlP depend on the local chemical orders around Si atoms. The valence-band maximum (VBM) is concave in energy between $y = 0$ and 1. In sharp contrast, the conduction-band minimum (CBM) energy is nearly constant for the whole range of y. To further demonstrate the asymmetric y dependence of the band-edge energies, we also considered a metastable phase at $y = 0.5$ in Fig. 1(c), which is 16 meV/atom less stable than the stable phase at the same y. Again, the two phases at $y = 0.5$ have almost the same energy for CBM, whereas the VBM of the metastable phase is substantially higher than that of the stable phase.

The asymmetric y dependence of the band-edge energies for the valence and conduction bands can be understood in terms of the symmetry breaking in the presence of the Al-P chains. The reduced symmetry leads to the level splitting of the $\Gamma_{25'}$-derived states at the valence-band edge, which would be threefold degenerate for a hypothetical "symmetric" Si_2AlP.

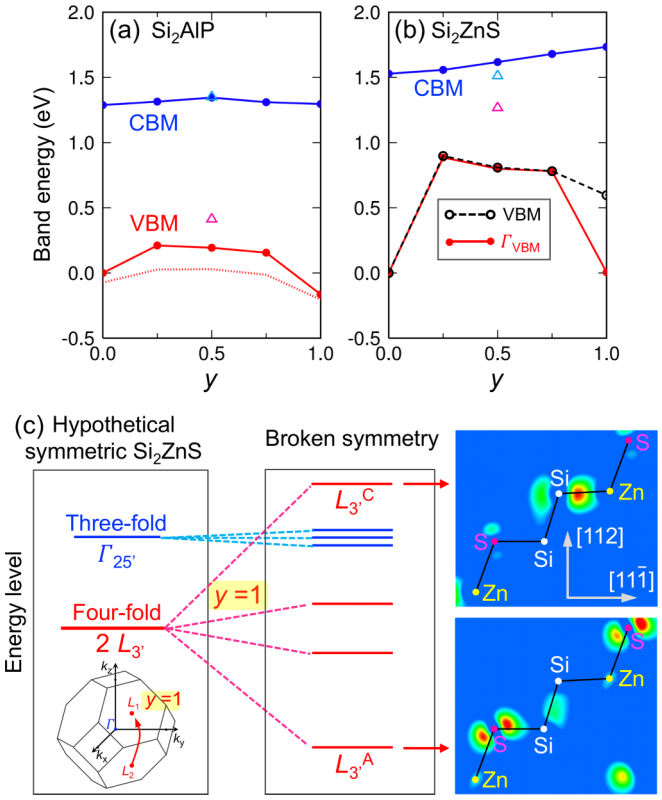

FIG. 3. Dependence of the band-edge energies of (a) Si_2AlP and (b) Si_2ZnS on the structural index y. For comparison, the results for the metastable phase in Fig. 1(c) are also shown in triangles. In (a), the average energies of the $\Gamma_{25'}$-derived valence-band states are plotted in a dotted line. (c) Schematic diagram showing how the valence-band-edge states of hypothetical symmetric Si_2ZnS are split as the symmetry is lowered in the presence of the Zn-S chains. For $y = 1$, two L points, L_1 and L_2, in the first Brillouin zone of Si are folded to the same k point (see inset), giving rise to the large level splitting of the $L_{3'}$-derived valence-band states. Charge density plots for $L_{3'}^C$ (top panel) and $L_{3'}^A$ (bottom panel) are also presented.

The energy difference of the split levels is 0.12 eV for y_0 and 0.09 eV for y_1. The level splitting is much larger for the mixed phases; for example, the energy splitting is 0.36 eV for the stable phase at $y = 0.5$, and it is further enhanced to 0.55 eV for the metastable phase at $y = 0.5$. The dotted line in Fig. 3(a) is a plot of the average energies of the $\Gamma_{25'}$-derived states. The upshift of the averaged band-edge energies is substantially reduced as compared to the case of the VBM, indicating that the large level splitting for the mixed phases contributes to the high VBM energies at the intermediate y values. For the conduction-band edge states, however, there is no such level-splitting effect. Furthermore, because of their different orbital symmetries, the Si-derived states in the conduction band do not strongly interact with the AlP-derived conduction-band states; for Si, the conduction-band states are the antibonding states of p orbitals, while the conduction band of AlP mainly has an s-orbital character [13]. Consequently, the CBM energy is relatively not sensitive to the local chemical orders around the Si atoms. Thus, the band-gap engineering in this class of materials is achieved by modifying the state near the VBM.

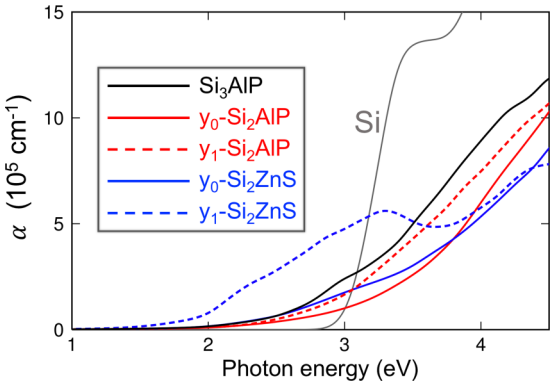

FIG. 4. Absorption coefficients of Si_2AlP and Si_2ZnS for different local chemical orders: $y = 0$ (solid line) and $y = 1$ (dotted line). For comparison, the results for Si and Si_3AlP are also included.

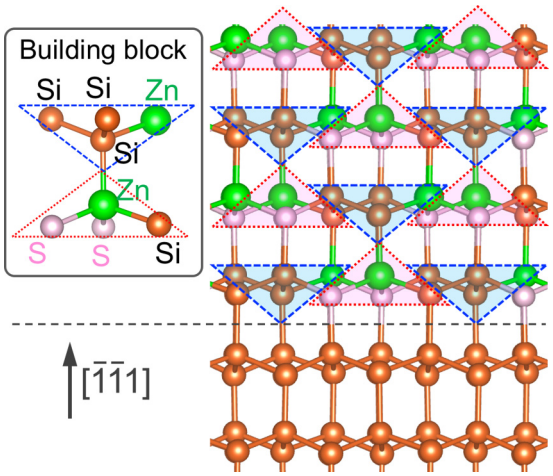

FIG. 5. Proposed interface structure between Si($\bar{1}\bar{1}1$) and the y_1 phase of Si_2ZnS. The inset shows the upper and lower building units that can be assembled to form the alloy phase on the epitaxial substrate.

A similar and more pronounced trend in the y-dependent band-edge energies was found for Si_2ZnS [Fig. 3(b)]. The valence-band edge at the Γ point at the endpoints, y_0 and y_1, are similar in energy, while for the intermediate y the band-edge energies are significantly shifted up. In contrast, the CBM energy has a nearly linear dependence on y. Unlike the case of Si_2AlP, at $y = 1$ the VBM of Si_2ZnS (dashed line) lies at a much higher energy than the valence-band edge at the Γ point (solid line). The explanation of the anomalously high VBM lies in the large level splitting of the $L_{3'}$-derived states at $y = 1$. For the y_1 phase, two L points, L_1 and L_2, in the first Brillouin zone of Si are folded to the same k point [Fig. 3(c)]. Because of the reduced symmetry, the fourfold $L_{3'}$-derived valence-band states split into four segregating levels [18], among which the highest energy level is localized on the Si-cation sublattice, while the lowest energy level is localized on the Si-anion sublattice. For Si_2AlP (not shown here), the energy splitting between the highest and lowest levels is 2.05 eV, which is still not large enough to push the highest $L_{3'}$-derived level above the $\Gamma_{25'}$-derived states. For Si_2ZnS, the level splitting of the $L_{3'}$-derived levels is much enhanced to 3.59 eV due to the large polarization of the group-II cation and the group-VI anion, making the highest $L_{3'}$-derived level lie 0.59 eV above the top of the $\Gamma_{25'}$-derived valence states [Fig. 3(c)]. The charge density plot in Fig. 3(c) indeed shows that for the highest level (labeled as $L^{C}_{3'}$) of the $L_{3'}$-derived states, the electron is distributed along the Si-Zn (i.e., cation) bonds that are perpendicular to the Si-Si atomic chains. In contrast, for the lowest level (labeled as $L^{A}_{3'}$), the electron is localized along the Si-S (i.e., anion) bonds. The different charge density distributions associated with the broken symmetry at $y = 1$ are responsible for the large energy splitting of the $L_{3'}$-derived states and hence the anomalously high VBM of Si_2ZnS.

Light-absorption properties of the Si_2AlP and Si_2ZnS alloys. In Fig. 4, the absorption spectra of Si_2AlP and Si_2ZnS are compared for different local chemical orders. Assuming polycrystalline alloy phases, we took an average of the components of the dielectric function along the x, y, and z axes to calculate the optical properties. We found that all the alloy phases with the composition $x = 0.5$ exhibit absorption at the photon energy below 3 eV, which is lacking for bulk Si. The y_1 phase of Si_2ZnS, which is a direct-band-gap semiconductor with the band gap of 1.22 eV, has considerably stronger low-energy absorption than the y_0 phase of the same material or the Si-Al-P systems such as Si_2AlP and Si_3AlP. In the visible range, the joint density of states is found to be similar for both phases of Si_2ZnS, only slightly larger for the y_1 phase. For the y_0 phase, which has an inversion symmetry in its atomic structure, the zone-folded optical transitions at the Γ point are parity forbidden for the visible range, leading to the relatively weak low-energy absorption of the y_0-Si_2ZnS. For the y_1 phase, however, the dipole-transition strength in the visible range is strong at and around the Γ point. A prior theoretical work [2] on a superlattice of alternating layers of two semiconductors (e.g., GaP/Si_2[001]) provides a useful insight into understanding the strong zone-folded optical transitions of y_1-Si_2ZnS compared to the Si-Al-P systems. Using a one-dimensional two-band tight-binding model, it was demonstrated that a superlattice system having a type-I alignment with large band offsets potentially has a strong oscillator strength for zone-folded transitions. If this argument could be generalized to a two-dimensional tight-binding model of the alloys in Fig. 1, the strong zone-folded transitions in Si_2ZnS might be attributed to the large band offsets of Si/ZnS (especially, the conduction-band offset) as compared to the offsets of Si/AlP.

Despite its strong absorption in the visible range, the proposed y_1 phase of Si_2ZnS poses a huge challenge for synthesis. Figure 5 depicts a possible interface structure between the alloy and a Si($\bar{1}\bar{1}1$) substrate. Note that the Zn-S and Si-Si atomic chains are parallel to the epitaxial substrate. The local chemical order changes only for the interfacial Si atoms that now have a local chemical environment of Si–Si_3Zn. The inset of Fig. 5 shows the building block of Si_2ZnS that consists of the upper and lower units. If there exist appropriate molecular precursors, the building units can be deposited on the Si substrate as shown in Fig. 5.

Another difficulty that could arise during the growth of Si_2ZnS is to avoid the formation of the y_0 phase, which is energetically more favored than the y_1 phase [Fig. 2(a)].

As we discussed earlier, the y_1 phase of Si_2ZnS has much higher VBM than the y_0 phase due to the symmetry-induced level splitting [Fig. 3(b)]. Therefore, it might be possible to enhance the relative stability of the y_1 phase by hole doping of the valence-band-edge state. Indeed, we found that the energy difference between the y_0 and y_1 phases gets reduced as the hole concentration increases [Fig. 2(c)]. Hence, local hole doping of the sample surface during the nonequilibrium growth could help synthesize the optically active y_1 phase. Another way to stabilize the y_1 phase is to utilize the electric dipoles of the Zn-S atomic chains, which are labeled as α and β depending on their orientations with respect to the [112] direction [Fig. 1(b)]. To synthesize the y_1 phase that consists of the atomic chains of a single type (say α), we could apply an electric field along the [112] direction during the growth of the alloys to make the α-type chains energetically more stable than the β-type chains.

III. CONCLUSION

In summary, we identified the atomic structures of covalent ($y = 0$), ionic ($y = 1$) and their mixed phases (intermediate y) for the nonisovalent Si_2AlP and Si_2ZnS alloys. We revealed the effects of the local chemical orders around the Si atoms on the stability and optoelectronic properties of Si_2AlP and Si_2ZnS, such as (i) the asymmetric y dependence of the band-edge energies for the valence and conduction bands, (ii) the anomalously high VBM for the y_1 phase of Si_2ZnS, and (iii) tunable relative stability of the alloy phases of Si_2ZnS through hole doping or applying electric field. The theoretical results highlighting the role of the local chemical orders in the nonisovalent alloys will provide useful insights into synthesizing a new class of Si-III-V and Si-II-VI alloys with improved optical properties.

ACKNOWLEDGMENTS

This work was supported by a National Research Foundation of Korea (NRF) grant funded by the Korea government (MSIP) (Grant No. 2016R1C1B2016046). Work at Beijing CSRC was supported by the National Key Research and Development Program of China (Grant No. 2016YFB0700700) and by the National Natural Science Foundations of China (Grants No. 51672023 and No. U1530401). Work at NREL was supported by the U.S. Department of Energy EERE SETP under Contract No. DOE DE - EE00025783.

[1] A. Polman, M. Knight, E. C. Garnett, B. Ehrler, and W. C. Sinke, Science **352**, 307 (2016).
[2] M. E. Lazzouni and L. J. Sham, Appl. Phys. Lett. **63**, 3253 (1993).
[3] X. Luo, S. B. Zhang, and S.-H. Wei, Phys. Rev. Lett. **89**, 076802 (2002).
[4] M. d'Avezac, J.-W. Luo, T. Chanier, and A. Zunger, Phys. Rev. Lett. **108**, 027401 (2012).
[5] T. Watkins, A. V. G. Chizmeshya, L. Jiang, D. J. Smith, R. T. Beeler, G. Grzybowski, C. D. Pweleit, J. Menéndez, and J. Kourvetakis, J. Am. Chem. Soc. **133**, 16212 (2011).
[6] J.-H. Yang, Y. Zhai, H. Liu, H. Xiang, X. Gong, and S.-H. Wei, J. Am. Chem. Soc. **134**, 12653 (2012).
[7] T. Watkins, L. Jiang, C. Xu, A. V. G. Chizmeshya, D. J. Smith, J. Menéndez, and J. Kouvetakis, Appl. Phys. Lett. **100**, 022101 (2012).
[8] L. Jiang, T. Aoki, D. J. Smith, A. V. G. Chizmeshya, J. Menéndez, and J. Kouvetakis, Chem. Mater. **26**, 4092 (2014).
[9] H. J. Xiang, B. Huang, E. Kan, S.-H. Wei, and X. G. Gong, Phys. Rev. Lett. **110**, 118702 (2013).
[10] Q. Wang, B. Xu, J. Sun, H. Liu, Z. Zhao, D. Yu, C. Fan, and J. He, J. Am. Chem. Soc. **136**, 9826 (2014).
[11] I.-H. Lee, J. Lee, Y. J. Oh, S. Kim, and K. J. Chang, Phys. Rev. B **90**, 115209 (2014).
[12] Y. J. Oh, I.-H. Lee, S. Kim, J. Lee, and K. J. Chang, Sci. Rep. **5**, 18086 (2015).
[13] P. Yu and M. Cardona, *Fundamentals of Semiconductors* (Springer-Verlag, Berlin, 2001).
[14] G. Kresse and J. Furthmüller, Phys. Rev. B **54**, 11169 (1996).
[15] P. E. Blöchl, Phys. Rev. B **50**, 17953 (1994).
[16] G. Kresse and D. Joubert, Phys. Rev. B **59**, 1758 (1999).
[17] J. Heyd, G. E. Scuseria, and M. Ernzerhof, J. Chem. Phys. **118**, 8207 (2003).
[18] J.-S. Park, J.-H. Yang, A. Kanevce, S. Choi, I. L. Repins, and S.-H. Wei, Phys. Rev. B **91**, 075204 (2015).